THE JOURNAL OF BIOLOGICAL CHEMISTRY VOL. 281, NO. 41, pp. 30365–30372, October 13, 2006

Structure and Dynamics of Membrane-associated ICP47, a Viral Inhibitor of the MHC I Antigen-processing Machinery*

Received for publication, March 29, 2006, and in revised form, June 26, 2006 Published, JBC Papers in Press, July 11, 2006, DOI 10.1074/jbc.M603000200

Christopher Aisenbrey[‡§1], Christina Sizun[§], Joachim Koch[¶], Meike Herget[¶], Rupert Abele[¶], Burkhard Bechinger[‡§2], and Robert Tampé[¶3]

From the [‡]Institut/Faculté de Chimie, Université Louis Pasteur/CNRS LC3-Unité Mixte de Recherche 7177, 4 Rue Blaise Pascal, Strasbourg 67070, France, [§]Max-Planck-Institute of Biochemistry, Am Klopferspitz 18A, 82152 Martinsried, Germany, and [¶]Institute of Biochemistry, Biocenter, Johann Wolfgang Goethe-University, Max-von-Laue-Strasse 9, 60438 Frankfurt am Main, Germany

To evade the host's immune response, herpes simplex virus employs the immediate early gene product ICP47 (IE12) to suppress antigen presentation to cytotoxic T-lymphocytes by inhibition of the ATP-binding cassette transporter associated with antigen processing (TAP). ICP47 is a membrane-associated protein adopting an α-helical conformation. Its active domain was mapped to residues 3–34 and shown to encode all functional properties of the full-length protein. The active domain of ICP47 was reconstituted into oriented phospholipid bilayers and studied by proton-decoupled ^{15}N and ^{2}H solid-state NMR spectroscopy. In phospholipid bilayers, the protein adopts a helix-loop-helix structure, where the average tilt angle of the helices relative to the membrane surface is $\sim 15^{\circ}$ ($\pm 7^{\circ}$). The alignment of both structured domains exhibits a mosaic spread of $\sim 10^{\circ}$. A flexible dynamic loop encompassing residues 17 and 18 separates the two helices. Refinement of the experimental data indicates that helix 1 inserts more deeply into the membrane. These novel insights into the structure of ICP47 represent an important step toward a molecular understanding of the immune evasion mechanism of herpes simplex virus and are instrumental for the design of new therapeutics.

Survival of vertebrates is strongly dependent on the adaptive immune system, which confers protection against pathogens or cancer. On the cellular level, the major histocompatibility complex (MHC)[4] class I-dependent pathway of antigen processing allows for presentation of antigenic peptides at the cell surface and can trigger the elimination of virus-infected or malignantly transformed cells by cytotoxic T lymphocytes (1–3). The efficiency of antigen presentation depends on the transporter associated with antigen processing (TAP), a member of the ATP-binding cassette protein family that translocates peptides generated by proteasomal protein degradation into the endoplasmic reticulum for loading onto MHC class I molecules (4). This process requires a macromolecular peptide-loading complex of ~1 MDa comprising the transporter subunits TAP1 and TAP2, the MHC class I heavy chain, the non-covalently associated β_2-microglobulin, the adaptor protein tapasin, and several auxiliary factors (5–9).

Herpes simplex virus type 1 is a highly abundant human pathogen that achieves lifelong persistence in the ganglia of the nervous system. Upon exogenous stimuli, it can be repeatedly reactivated and infect related mucosal tissues leading to clinical symptoms (10). To escape immune surveillance, herpes simplex virus compromises the host's cytotoxic T lymphocyte response via ICP47, an 88-amino-acid immediate early gene product (IE12) that blocks TAP function (11–15). In the absence of a functional TAP transporter (within 3 h of infection with herpes simplex virus), peptide loading onto MHC class I molecules is inhibited, and as a consequence, empty MHC I molecules are retained in the endoplasmic reticulum and ultimately directed to proteasomal degradation. By binding with nanomolar affinity to the heterodimeric TAP complex, ICP47 blocks peptide binding but not ATP binding to the ATP-binding cassette transporter (12, 15). Functional studies with N- and C-terminally truncated variants of ICP47 demonstrate that the N-terminal domain of ICP47 is sufficient for TAP inhibition (residues 1–53 (16), 2–35 (17), and 3–34 (18)). Moreover, by alanine scanning mutagenesis, three regions (residues 8–12, 17–24, and 28–31) were identified within the active domain of ICP47, which are critical for TAP inhibition (17). The active domain of ICP47 (residues 3–34) displays an identical ability to inhibit TAP function when compared with the full-length protein, illustrating preservation of the functional properties (18).

The secondary structure and membrane association of ICP47 have been analyzed by circular dichroism spectroscopy and tryptophan fluorescence quenching (16). Both, full-length ICP47 as well as the active domain are mainly unstructured in aqueous solution independent of the protein concentration or pH value (16), which is in accordance with the observation that purification in organic solvent or heating to 100 °C has no effect on its ability to inhibit TAP (15, 18). However, after binding to phospholipid membranes, a transition to helical conformations is induced in the active domain as well as in the full-length protein, confirming a tight membrane interaction (16). Multidimensional solution NMR spectroscopy indicates that the

* This work was supported by the Agence Nationale pour la Recherche contre le Syndrome d'Immunodéficience Acquise and the Deutsche Forschungsgemeinschaft (SFB 628). The costs of publication of this article were defrayed in part by the payment of page charges. This article must therefore be hereby marked "*advertisement*" in accordance with 18 U.S.C. Section 1734 solely to indicate this fact.

[1] Present address: Dept. of Biophysical Chemistry, Umeå University, 90187 Umeå, Sweden.

[2] To whom correspondence may be addressed. Fax: 33-390-24-51-51; E-mail: bechinger@chimie.u-strasbg.fr.

[3] To whom correspondence may be addressed. Fax: 49-69-798-29495; E-mail: tampe@em.uni-frankfurt.de.

[4] The abbreviations used are: MHC, major histocompatibility complex; ICP, infected cell protein; TAP, transporter associated with antigen processing; ppm, parts/million.

active domain of ICP47 adopts a helix-loop-helix conformation in the presence of detergent micelles, where helix 1 comprises residues 4–15 and helix 2 residues 22–32. However, it should be noted that considerable differences have been observed in the past when the structural details of polypeptides obtained in the presence of detergents or when associated with bilayers are compared with each other. For example, the possibility exists that the helix-turn-helix structure observed in micelles is an artifact of the geometry and the high curvature of such environments. Furthermore, it would be of interest to know how the helical domains align relative to the bilayer surface. The answer to such questions can only be obtained by investigating the structure of ICP47 when associated with planar phospholipid bilayers.

Solid-state NMR spectroscopy is an emerging technique in the study of the structure and dynamics of membrane-associated proteins and peptides (19–22). Although *a priori* NMR interactions strongly depend on the alignment of the molecules relative to the magnetic field direction, in isotropic solutions, fast rotational diffusion results in averaging, and therefore only the isotropic chemical shift values as well as direct spin-spin couplings are observed. In contrast, in static solid samples or in samples where averaging is anisotropic, the most pronounced features of the spectra can be attributed to this orientational dependence of NMR interactions. When uniaxially oriented samples are investigated by static solid-state NMR spectroscopy, advantage is taken of this orientation dependence of NMR interactions, which allows extraction of angular constraints for structural analysis. Proton-decoupled ^{15}N solid-state NMR spectroscopy has been shown to be particularly useful in providing detailed information on the helical tilt angles and therefore the topology of membrane-associated polypeptides in a direct manner (23). In the case of polypeptides that have been isotopically labeled with ^{15}N at one of their amide bonds and reconstituted into bilayers oriented with their normal parallel to the magnetic field direction, ^{15}N chemical shifts in the 200-ppm range are indicative of transmembrane helix alignments, whereas in-plane-oriented helices resonate at $<$100 ppm (24). This is illustrated in the *top panel* of Fig. 2.

Deuterium solid-state NMR spectroscopy provides complementary angular restraints, which in combination with the ^{15}N chemical shift allow for the accurate determination of the tilt and azimuthal angles of membrane-associated helices (24). The deuterium quadrupole splitting of alanines carrying three deuterons at the methyl group has been shown to be a very sensitive indicator of helix alignments, which permits the tracking of even small topological changes (24). Furthermore, the ^{2}H NMR technique has recently been developed to monitor the mosaic spread of helix alignments and the rotational diffusion of membrane polypeptides (24, 25).

Here ^{2}H and proton-decoupled ^{15}N solid-state NMR spectroscopy have been combined to investigate in considerable detail the alignment, limits, and mosaic spread of the secondary structural elements of reconstituted ICP47 in oriented phospholipid bilayers. By positioning at strategic places eight different isotopic labels within the ICP47 sequence, it was not only possible to test for the existence of a helix-loop-helix conformation also in phospholipid bilayers, but even more important, the alignment of the helical domains relative to the membrane surface could be determined. Furthermore, a novel Edmundson helical wheel-based "energy minimization" strategy was developed for this study to select, among a number of topological states, the one that agrees with the oriented solid-state NMR data. The structural and topological information derived from these measurements provide detailed insights into the inhibition mechanism of ICP47.

EXPERIMENTAL PROCEDURES

Peptide Transport Assays—Assays were performed with microsomes isolated from Raji cells (human Burkitt lymphoma). Microsomes (50 μg of total protein) were pre-incubated with 10 μM ICP47-(2–34) for 20 min on ice. After the addition of MgATP (3 mM) or apyrase (1 unit) and radiolabeled peptide (460 nM, RRYQNSTEL; *N*-core glycosylation-targeting site underlined), transport was performed for 2 min at 32 °C. The reaction was stopped by the addition of 1 ml of cold phosphate-buffered saline buffer supplemented with 10 mM EDTA. After centrifugation, microsomes were solubilized in 1 ml of lysis buffer (50 mM Tris/HCl, 150 mM NaCl, 5 mM KCl, 1 mM $CaCl_2$, 1 mM $MnCl_2$, 1% Nonidet P-40, pH 7.5) for 20 min on ice. Insoluble debris was removed by centrifugation, and glycosylated peptides in the supernatant were bound to concanavalin A-Sepharose beads for 16 h at 4 °C. After washing three times with lysis buffer, radioactivity associated with the beads was quantified by gamma counting (26). Peptides were radiolabeled with $Na^{125}I$ as reported previously (27).

ICP47 Binding Assays—TAP-containing membranes or purified TAP were incubated with increasing concentrations of ICP47-(2–34) for 60 min at 4 °C in 50 μl of binding buffer A (20 mM Hepes, 140 mM NaCl, 15% glycerol, pH 7.4) or binding buffer B (20 mM Hepes, 140 mM NaCl, 15% glycerol, 0.1% digitonin, pH 7.4), respectively. Radiolabeled peptide RR(^{125}I)YQKSTEL was added to a final concentration of 200 nM and incubated for 15 min at 4 °C. Unbound peptides were removed by washing the membranes or purified protein with 200 μl of ice-cold binding buffers using a vacuum manifold with 96-well filter plates (MultiScreen, 1-μm glass fiber Type B filter, Millipore). The amount of peptide bound to the filters was quantified by gamma counting. Background binding was determined in the presence of a 200-fold excess of unlabeled peptide RRYQKSTEL. The binding constant of ICP47-(2–34) was derived from the inhibition data by using heterologous competition with ligand depletion as the fitting procedure with the program Prism® (GraphPad Software, Inc.). The affinity of RRYQKSTEL was set to 30 nM as determined by equilibrium binding; the specific activity of the peptide was 40 counts/min/fmol, and the 200 nM radiolabeled peptide in 50 μl of reaction volume had an activity of 400,000 counts/min.

Peptide Synthesis and Isotope Labeling—ICP47-(2–34), Ac-SWALEMADTFLDNMRVGPRTYADVRDEINKRGR-NH_2, was synthesized by solid-phase synthesis using Fmoc (*N*-(9-fluorenyl)methoxycarbonyl) chemistry. At the underlined positions, isotope-labeled amino acids were incorporated in the following manner. In a first set, polypeptides labeled at a single site with ^{15}N at either position Ala^{8} or Ala^{23} were prepared. To test in more detail the alignment of the second helix encompassing residues 22–31 (28), the functionally active mutant D27A (18)

was labeled with [^{15}N]alanine at the modified position. In a second set, ICP47 analogues that are simultaneously enriched at the backbone with ^{15}N and with a [$^{2}H_3$]alanyl residue were prepared. The double labeling patterns were [^{15}N]Gly^{18}/[$^{2}H_3$]Ala^{27} (D27A) and [^{15}N]Val^{17}/[$^{2}H_3$]Ala^{8}. The synthetic products were purified by a C_{18} reversed-phase high pressure liquid chromatography column (Vydac). The identity of the products was confirmed by analytical high pressure liquid chromatography and matrix-assisted laser desorption ionization mass spectrometry.

NMR Sample Preparation—Phospholipids were purchased from Avanti Polar Lipids (Birmingham, AL). 10 mg of peptide and 200 mg of 1-palmitoyl-2-oleoyl-*sn*-glycero-3-phosphatidyl choline (or 1-palmitoyl-2-oleoyl-*sn*-glycero-3-phosphatidylcholine/1-palmitoyl-2-oleoyl-*sn*-glycero-3-phosphatidylserine 3:1 mol/mol; spectra not shown) were co-dissolved in 2.5 ml of trifluoroethanol and 0.2 ml of water. The mixtures were applied onto 30 ultrathin cover glasses (9 × 22 mm; Paul Marienfeld GmbH & Co. KG, Lauda-Königshofen, Germany) first dried in air and thereafter in high vacuum overnight. After equilibration at 93% relative humidity, the glass plates were stacked on top of each other. The stacks were stabilized and sealed with Teflon tape and plastic wrappings. The sample alignment was routinely controlled using proton-decoupled ^{31}P solid-state NMR spectra as described previously (24, 29).

NMR Measurements—Solid-state NMR spectra were recorded on a Bruker Avance wide bore NMR spectrometer operating at 9.4 teslas. A commercial double-resonance solid-state NMR probe modified with flattened coils of dimensions 15 × 4 × 9 mm was used (30). The spectra of samples rotated by 90° relative to the magnetic field directions were acquired using a second coil of similar geometry. Proton-decoupled ^{15}N solid-state NMR spectra were acquired using cross-polarization (31, 32). Typical acquisition parameters were the following: spin lock time 1.6 ms, recycle delay 3 s, ^{1}H B_1 field 31 kHz, 256 data points, 20,000–40,000 acquisitions, and spectral width 40 kHz. Before Fourier transformation, an exponential apodization function corresponding to a line broadening of 300 Hz was applied. NH_4Cl (41.5 ppm) was used as a reference corresponding to ~0 ppm for liquid NH_3.

Deuterium solid-state NMR spectra were recorded using a quadrupolar echo pulse sequence (33) with the following parameters: ^{2}H B_1 field 50 kHz, inter-pulse delay 50 μs, spectral width 100 kHz, 4096 data points, 40,000 scans, and a repetition time of 1.5 s. The spectra were referenced relative to $^{2}H_2O$ (0 ppm). An exponential apodization function corresponding to a line broadening of 300 Hz was applied before Fourier transformation.

Calculation of Orientational Restraints—To evaluate the peptide orientations, a Cartesian coordinate system was defined. The long axis of the α-helix defines the *z*-axis, and the *y*-axis resides within the plane dividing hydrophobic and hydrophilic sections of amphipathic helices, such as those found in the ICP47 structure in micellar environments (28). The computer program Insight II (BIOSYM, Molecular Simulations, San Diego, CA) was used to generate Protein Data Bank (PDB) data sets of the oriented helices. The PDB structural data file was used to extract the coordinates of the labeled ^{15}N atoms and its neighbors (NH and C atom of the previous amino acid).

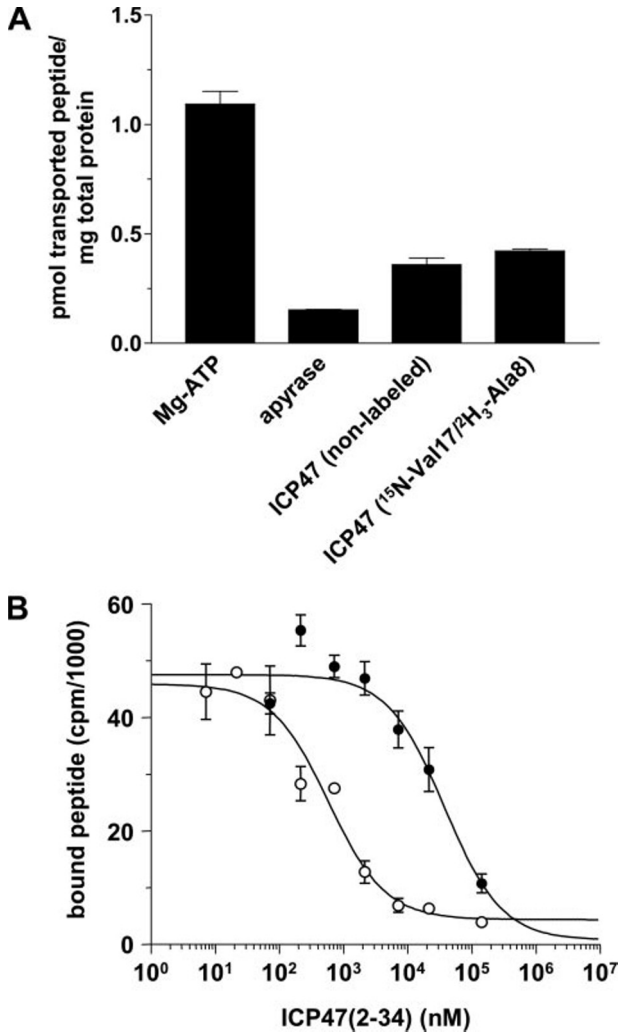

FIGURE 1. **Viral inhibition of TAP-dependent peptide binding and transport.** *A*, microsomes isolated from Raji cells were used in transport assays with radiolabeled peptide (RRYQNSTEL) in the presence of ATP, apyrase, or ATP and a 20-fold molar excess of non-labeled and [^{15}N]Val^{17}/[$^{2}H_3$]Ala^{8}-labeled ICP47-(2–34), respectively. Peptide translocation was performed for 2 min at 32 °C. Transported peptides were quantified by gamma counting in triplicate experiments. *B*, the binding affinity of the active domain of ICP47 (*ICP47-(2–34)*) to TAP within the membrane (*open circles*) or purified, digitonin-solubilized TAP (*closed circles*) derived from insect cells was determined in competition experiments with a radiolabeled peptide epitope. TAP was pre-incubated with increasing concentrations of ICP47-(2–34) for 60 min at 4 °C. Subsequently, binding was assayed by adding 200 nM radiolabeled peptide (RRYQKSTEL) for 15 min at 4 °C. The amount of peptide bound to the TAP complex was quantified by gamma counting in triplicate measurements. *cpm*, counts/min.

The coordinates of the labeled peptide bonds were needed to calculate the ^{15}N chemical shift tensor in this reference frame using information on ^{15}N chemical shift tensors reported in the literature (34), where the main tensor elements exhibit values of 223, 75 and 61 ppm. By successively rotating the peptide molecule around the *z*- (pitch angle) and the *y*-axis (tilt angle) the three-dimensional orientational space was systematically screened in 50 × 50 steps using a program written in MATHEMATICA (24). Contour plots mark the angular pairs that agree with the experimental results. The simulation of the ^{2}H solid-state NMR spectra was performed on the same principles and has been described previously (24).

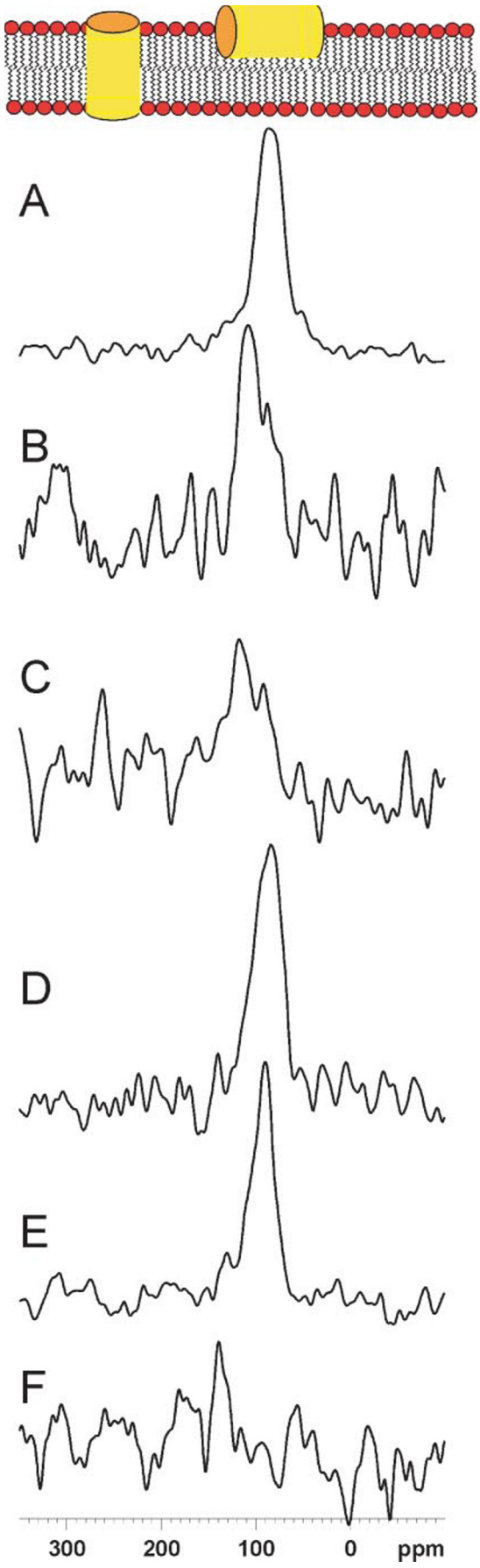

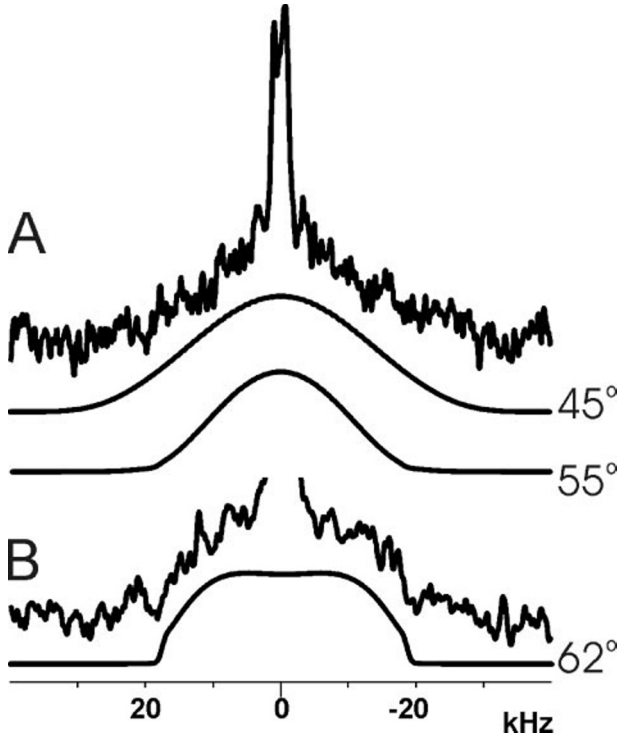

FIGURE 3. **^2H solid-state NMR spectra of ICP47-(2–34) labeled with $^2H_3$ at position Ala^8 (*A*) or Ala^{27} (*B*).** The samples are aligned with the membrane normal parallel to the magnetic field direction. Underneath the spectra are simulations of the deuterium line shapes resulting from alignments of the C_α–C_β bonds relative to the magnetic field direction of 45 or 55° for Ala^8 and 62° for Ala^{27}, respectively. The mosaic spread is ±10° for both sites.

Similarly, the coordinates of the C_α atoms were extracted from oriented PDB files. From these coordinates, the center of the mass of the C_α atoms for each of the respective helices 5–16 and 22–31 was calculated to define the center of a new coordinate system. The coordinates thus established were also used for an analysis of the positioning of amino acid residues relative to the hydrophobic-hydrophilic interface. During these calculations, the insertion depth d_{ins} was simulated by a corresponding shift of the z coordinates. The z coordinates were then scaled with the following factor.

$$C_z = 0.5 - \frac{1}{1 + 10^{z-15.75}} \qquad \text{(Eq. 1)}$$

In this manner, it was possible to model a membrane of 27 Å hydrophobic thickness and an interface extending over 4–5 Å (35). The values thus obtained are multiplied with the hydrophobic index of the individual amino acid side chains (36) and summed up to provide a total index for the hydrophobic effect I_{hydro} that is associated with the peptide alignment and insertion depth. The graphs (see Fig. 4, *A* and *B*, and Fig. 5) represent the configurations of penetration depth, tilt, and pitch angle where I_{hydro} is minimal.

FIGURE 2. **Proton-decoupled ^{15}N solid-state NMR spectra of ICP47-(2–34) labeled with ^{15}N at position Ala^8 (*A*), Val^{17} (*B* and *F*), Gly^{18} (*C*), Ala^{23} (*D*), and Ala^{27} (*E*).** Spectra *A*–*E* were recorded at sample alignments with the membrane normal parallel to the magnetic field direction and spectrum *F* after the sample had been tilted by 90°. The correlation between the ^{15}N chemical shift and helix alignments is illustrated on *top* of *panel A*.

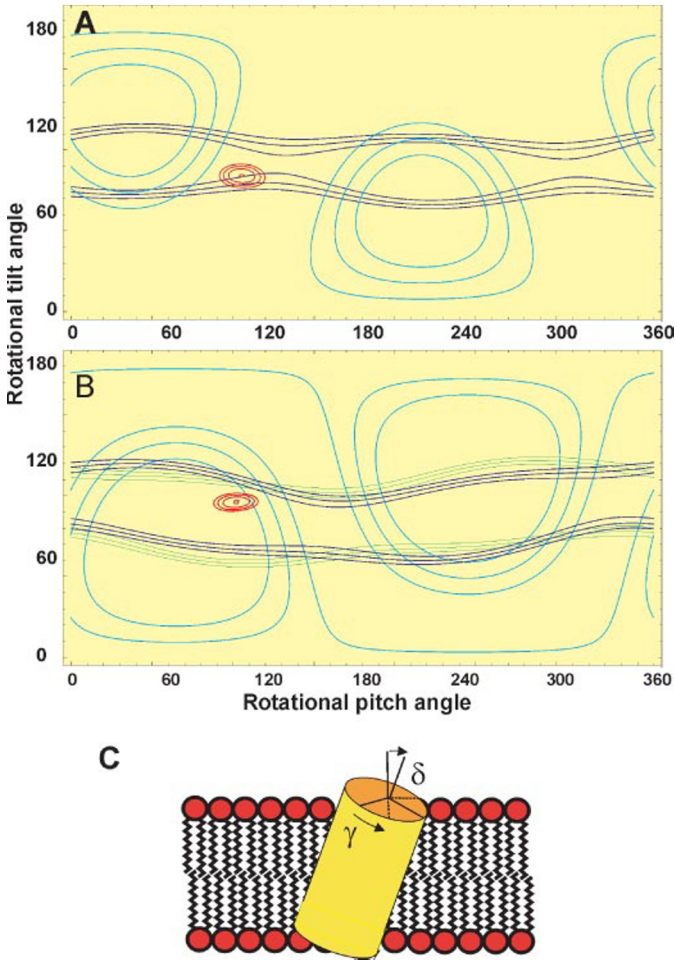

FIGURE 4. Shown are the contour plots of the tilt and rotation pitch angles of helices 1 (*A*) and 2 (*B*). The contours are calculated from the orientation-dependent ^{15}N chemical shift and ^{2}H quadrupolar splitting data of Ala^{8} (*A*) as well as the Ala^{23} and Ala^{27} positions (*B*). The *lines* in *dark blue* represent angular restraints obtained from the ^{15}N chemical shift measurements (±5 ppm) of position 8 and 27, and the *green lines* represent that of position 23. Angular restraints obtained from ^{2}H NMR measurements are shown in *light blue* (Ala^{8}, 55 ± 10°; and Ala^{27}, 62 ± 10°) (Fig. 3). The *red circles* are indicative of the tilt and rotational pitch angles that result from a three-dimensional hydrophobic index analysis (see "Experimental Procedures" for details). For a bilayer of 31.5 Å hydrophobic thickness and an interface of 4.5 Å, the positioning is optimized when the distance from the membrane interior to the center of the mass of helix 1 is 15.5 Å and that of helix 2 is 17.5 Å. *C*, model illustrating the tilt angle δ and the rotational pitch angle γ.

RESULTS AND DISCUSSION

Solution NMR investigations have shown that the active domain of ICP47 adopts α-helical secondary structures encompassing residues 4–15 and 22–32 in the presence of SDS micelles (28). To investigate for the first time the structure of this potent immune evasin in the bilayer-associated state, ICP47-(2–34) was synthesized by solid-phase chemistry, and ^{15}N and ^{2}H isotopic labels were incorporated at single sites.

The isotope-labeled active domain of ICP47-(2–34) ([^{5}N]Val^{17}/[$^{2}H_3$]Ala^{8}) was first examined for its ability to inhibit TAP-dependent peptide translocation in microsomes isolated from human Burkitt lymphoma (Raji) cells. As expected, the isotope-labeled active domain of ICP47 displayed the same ability to inhibit TAP when compared with its non-labeled counterpart, demonstrating that the labeling had no adverse effects on the properties of the domain (Fig. 1*A*).

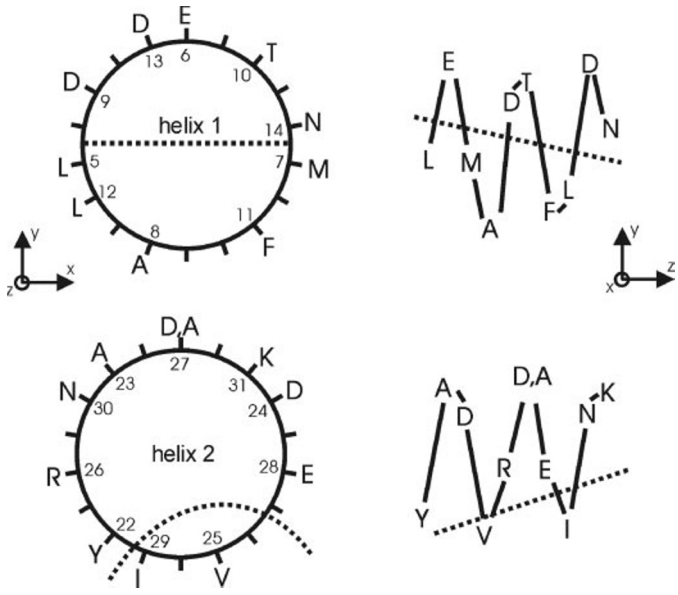

FIGURE 5. **Edmundson helical wheel diagrams of ICP47 helices.** Residues 5–16 (helix 1) and 22–31 (helix 2) are shown in their classical representation. The *side view* projections indicate the distribution of hydrophobic and hydrophilic residues when the helices are inclined relative to the membrane surface (*dotted lines*). The coordinate system used during analysis of solid-state NMR spectra is indicated *next to* helix 1.

We next examined whether the active domain of ICP47 requires a lipid environment to interact efficiently with the TAP complex. We thus performed competition binding experiments with purified, digitonin-solubilized TAP or membrane-bound TAP employing the active domain of ICP47 and the radiolabeled peptide RR(^{125}I)YQKSTEL. Solubilized TAP, as well as TAP within the membrane, displays the same affinity (K_D = 30 nM).[5] The TAP samples were pre-incubated with graded amounts of ICP47-(2–34) and subsequently probed with radiolabeled peptide. Peptides bound to TAP were quantified by γ-counting. Strikingly, the inhibition constant (K_i) of ICP47 for the solubilized TAP complex (K_i = 5093 nM) is 65 fold higher than that for TAP within the membrane (K_i = 79 nM) (Fig. 1*B*). These results demonstrate that ICP47 requires a lipid environment to bind with high affinity to the TAP heterodimer. Notably, the amount of functional heterodimeric TAP complexes was identical in both sets of experiments as indicated by the same peptide binding value in the absence of ICP47 (Fig. 1*B*, see *converging intersection*).

To determine the structure of the active domain of ICP47 in the membrane-bound state, isotopically labeled ICP47-(2–34) was reconstituted into oriented phospholipid bilayers and investigated by ^{2}H- and proton-decoupled ^{15}N solid-state NMR spectroscopy. The macroscopic phase properties and the membrane alignment were routinely controlled by proton-decoupled ^{31}P solid-state NMR spectroscopy on the same samples (data not shown). Fig. 2 shows the proton-decoupled ^{15}N solid-state NMR spectra of ICP47-(2–34) in oriented phospholipid bilayers. The Ala^{8}, Ala^{23}, and Ala^{27} positions all show chemical shift values between 85 and 89 ppm (Fig. 2; *A*, *D*, and *E*) indicative of helix alignments approximately parallel to the mem-

[5] M. Herget, R. Abele, and R. Tampé, unpublished data.

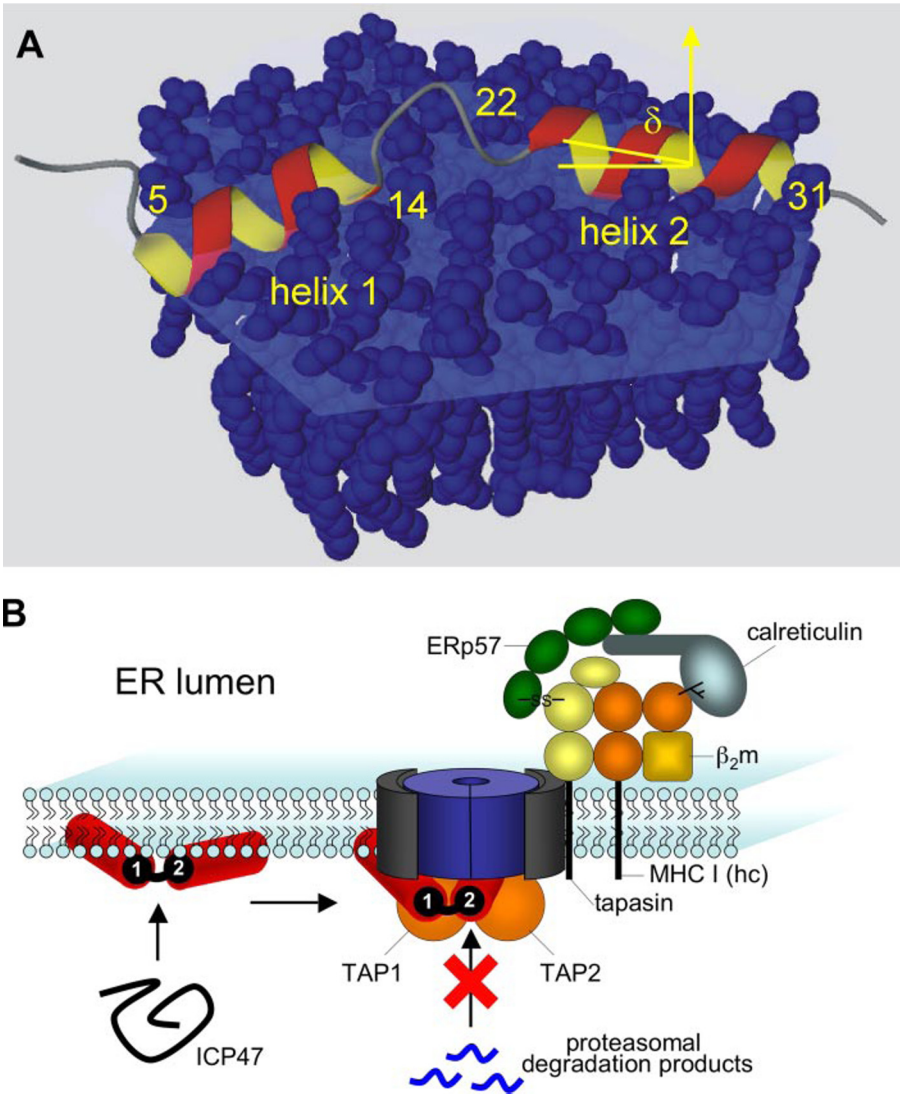

FIGURE 6. **Model of the active domain of ICP47 in phospholipid bilayers.** *A*, the bilayer normal (*arrow*) and the tilt angle δ for helix 2 are indicated. MOLMOL software was used to prepare this figure (38). *B*, after binding to the cytosolic face of the endoplasmic reticular (*ER*) membrane, ICP47 adopts a helix-loop-helix conformation. Subsequent association with the peptide-loading complex at the lipid-TAP interface blocks the peptide supply to MHC class I molecules. The peptide-loading complex consists of the ATP-binding cassette half-transporter subunits TAP1 and TAP2, the adaptor protein tapasin, the MHC class I heavy chain (*hc*), the non-covalently associated β_2-microglobulin (β_2m), and several auxiliary factors (*e.g.* calnexin and the thiol-oxidoreductase ERp57) (8).

brane surface (23). In contrast, the [^{15}N]Val^{17} position exhibits a well defined ^{15}N chemical shift of 108 ppm, a value close to the isotropic chemical shift position (*i.e.* indicative of a lack of orientation; Fig. 2*B*).

To investigate the orientation and dynamics of this helix in further detail, the same sample was rotated by 90° (25). In this arrangement, the long axis of an in-plane-oriented α-helix can adopt all angles between 0 and 360° relative to the magnetic field direction. *A priori,* the ^{15}N chemical shift is therefore expected to vary over a wide range within the limits of 60 and 230 ppm. However, in the case of fast rotational diffusion around the membrane normal, the observed ^{15}N chemical shift exhibits a mean value corresponding to $\sigma_\perp$ of the averaged chemical shift tensor (23, 25). The value observed for the Val^{17} position was 138 ppm (Fig. 2*F*) and different from the ^{15}N chemical shift observed at alignments of the sample normal parallel to the magnetic field direction (Fig. 2*B*). Therefore, the ensemble of ^{15}N chemical shift data indicates a significant amount of non-isotropic averaging at this site. Relatively weak signal intensities were obtained for the Gly^{18} position at ~117 ± 5 ppm (Fig. 2*C*). In the presence of fast motions, the concomitant reduction of the active ^{1}H-^{15}N dipolar interactions reduces the efficiency of the cross-polarization technique, which allows for the transfer of magnetization from the abundant ^{1}H to the less sensitive ^{15}N nuclei. As a result, weak ^{15}N signal intensities close to the isotropic values were observed for these mobile sites. The solid-state NMR data thereby reflect well the structure observed in micellar environments, where Ala^8 is part of the first helix followed by a flexible loop region encompassing Val^{17} and Gly^{18} and a second helix including Ala^{23} and Glu/Ala^{27}. However, when the chemical shift positions are analyzed in more detail, it becomes obvious that, in lipid bilayers, the Val^{17} site is less flexible when compared with Gly^{18}. Collectively, the solid-state NMR data confirm a helix-loop-helix conformation, where the helices are aligned approximately parallel to the membrane surface.

Additional deuterium NMR spectra were obtained from the $^2H_3$-labeled alanines at positions 8 or 27 (Fig. 3). It has been shown previously that the deuterium NMR quadrupole splitting is very sensitive to the alignment of the C_α–C_β vector relative to the magnetic field direction (24). The data therefore provide additional orientational restraints (Fig. 4). Furthermore, the deuterium NMR line shape is sensitive to the orientational mosaic spread of helix domains. By comparison to theoretical line shapes, a mosaic spread of the deuterium-labeled alanine C_α–$C_\beta{}^2H_3$ bond of 10° is estimated, indicating that the peptide helices exhibit a considerable degree of motion that results in a broadened distribution of tilt and rotational pitch angles. A quantitative evaluation of the ^{15}N chemical shift data indicates a tilt angle in the range between 64 and 88° for helix 1 encompassing Ala^8 (Fig. 4*A*). The ^{2}H data provide valuable information not only about the helix mosaic spread (see above), but the resulting line shape also limits the range of possible helix alignments relative to the membrane normal (Fig. 3*A*). The combination of both data sets therefore confines the helix alignment to six regions on the tilt/pitch angle topological map shown in Fig. 4*A*.

When the data of helix 2 are analyzed in a quantitative manner, the orientational restraints of positions 23 and 27 overlap, thereby defining four regions where the orientational pairs (tilt/pitch angle) agree with both ^{15}N chemical shift measurements. These are located around 63/166, 106/118, 74/295, and 117/348° (Fig. 4*B*). Of those pairs, the first and last as well as the second and third are symmetry-related, corresponding to helices associated with either the top or the bottom monolayer. Of those results, only the second and third angular pair also fit the ^{2}H solid-state NMR data.

In a next step, we refined these results by evaluating the energies associated with the insertion of the helices in the hydrophobic-hydrophilic environment of the membrane interface using an extension of the Edmundson helical wheel analysis. The helical wheel diagram allows one to view the amphipathic distribution in the projection of the helix long axis and thus to evaluate the rotational pitch angle and the penetration depth of a given helix. In this work, a third dimension representing the peptide tilt angle was introduced for the analysis. Such an energy minimization protocol indicates a tilt angle of 84° and a rotational pitch angle of 106° for helix 1 (Fig. 4*A*) in proximity of the region around 75/72°, which was identified by our experimental data. The small deviation is probably a result of the calculations not taking into account atomic models of phospholipids or peptide conformational flexibility. When the same analysis is performed with the structural coordinates of helix 2, which have previously been obtained from the NMR structural analysis of ICP47 in detergent micelles and deposited in the PDB data base (28), the most favorable alignment is 95/102° (Fig. 4*B*). This topological coordinate corresponds closely to the second angular pair identified experimentally (106°/118°). The data therefore indicate that the average tilt angle of the helices deviates from perfect in-plane alignments by ~15° (±7°). These findings are represented by helix projection diagrams in Fig. 5. Notably, the calculations also suggest that the penetration depth of the two helices, when considering their centers of mass, is different by 2 Å.

In agreement with these solid-state NMR data, several lines of biochemical evidence demonstrate that this α-helical conformation of ICP47 in the membrane-bound state is a prerequisite for TAP inhibition. First, truncation of the helix 1 leads to a complete inactivation of the inhibitor and failure to induce an α-helical conformation (16). These data show that key sequence elements in the active domain are essential for both membrane association and TAP inhibition. Second, insertion of a proline at position 11 breaking helix 1 causes a drastic loss of activity, illustrating the functional impact of the formation of an α-helical conformation (18). Third, fluorescence quenching experiments suggest that the single tryptophan located at position 3 is in contact with the lipid environment, thus demonstrating that the active domain of ICP47 interacts with the membrane (16). Most importantly, within the current study, we have demonstrated, based on competition binding experiments, that a lipid environment is a prerequisite for high affinity binding of ICP47 to the heterodimeric TAP complex (Fig. 1*B*). Without a membrane, the binding affinity of ICP47 was reduced by almost two orders of magnitude.

A structural model summarizing the data discussed above is shown in Fig. 6. The solid-state NMR data reveal a flexible loop region separating two helical domains, which exhibit small deviations from perfect in-plane alignments and considerable mosaic spread. Theoretical considerations suggest that helix 1 inserts more deeply into the hydrophobic interior of the membrane (Fig. 6*A*). This first structural model of ICP47 in its bilayer-associated state provides important insights into the structure and topology of membrane-bound ICP47, which are instructive in understanding how and where ICP47 binds to the heterodimeric TAP complex. Based on the data presented, the active domain interacts with TAP at the subunit-membrane interface within the lipid head group region and blocks peptide translocation into the endoplasmic reticular lumen (Fig. 6*B*). Previous studies have demonstrated that both TAP subunits are required for ICP47 binding (12, 15, 26). In combination with similar observations for the partitioning at various peptide hormone receptors (37), the N-terminal region, with particular emphasis on helix 1 of ICP47, might serve as a membrane anchor to locally concentrate the inhibitor at the TAP complex, thus increasing the efficiency of the inhibition process.

In the membrane-bound state, ICP47 escapes proteasomal degradation, which otherwise occurs rapidly in the membrane-free state.[6] The presented structural model of ICP47 corresponds to a conformation, which is adopted just before or concurrently with the functional association with the TAP heterodimer, circumventing a disfavored soluble intermediate. This represents an elegant and so far unforeseen strategy of peptidic effectors and unstructured regions in avoiding degradation by the proteasome.

Acknowledgments—We thank Dr. Karl-Heinz Wiesmüller (EMC microcollections, Tübingen, Germany) for support in peptide synthesis and Dr. Clemens Glaubitz for helpful comments on the manuscript.

REFERENCES

1. Yewdell, J. W., and Haeryfar, S. M. (2005) *Annu. Rev. Immunol.* **23,** 651–682
2. Grommé, M., and Neefjes, J. (2002) *Mol. Immunol.* **39,** 181–202
3. Lehner, P. J., and Cresswell, P. (2004) *Curr. Opin. Immunol.* **16,** 82–89
4. Abele, R., and Tampé, R. (2004) *Physiology* (*Bethesda*) **19,** 216–224
5. Antoniou, A. N., Ford, S., Pilley, E. S., Blake, N., and Powis, S. J. (2002) *Immunology* **106,** 182–189
6. Bangia, N., and Cresswell, P. (2005) *Immunology* **114,** 346–353
7. Koch, J., Guntrum, R., Heintke, S., Kyritsis, C., and Tampé, R. (2004) *J. Biol. Chem.* **279,** 10142–10147
8. Koch, J., and Tampé, R. (2006) *Cell. Mol. Life Sci.* **63,** 653–662
9. Ortmann, B., Copeman, J., Lehner, P. J., Sadasivan, B., Herberg, J. A., Grandea, A. G., Riddell, S. R., Tampé, R., Spies, T., Trowsdale, J., and Cresswell, P. (1997) *Science* **277,** 1306–1309
10. Whitley, R. J., Kimberlin, D. W., and Roizman, B. (1998) *Clin. Infect. Dis.* **26,** 541–553
11. York, I. A., Roop, C., Andrews, D. W., Riddell, S. R., Graham, F. L., and Johnson, D. C. (1994) *Cell* **77,** 525–535
12. Ahn, K., Meyer, T. H., Uebel, S., Sempe, P., Djaballah, H., Yang, Y., Peterson, P. A., Früh, K., and Tampé, R. (1996) *EMBO J.* **15,** 3247–3255
13. Früh, K., Ahn, K., Djaballah, H., Sempe, P., van Endert, P. M., Tampé, R.,

[6] R. Tampé, unpublished observations.

Peterson, P. A., and Yang, Y. (1995) *Nature* **375,** 415–418
14. Hill, A., Jugovic, P., York, I., Russ, G., Bennink, J., Yewdell, J., Ploegh, H., and Johnson, D. (1995) *Nature* **375,** 411–415
15. Tomazin, R., Hill, A. B., Jugovic, P., York, I., van Endert, P., Ploegh, H. L., Andrews, D. W., and Johnson, D. C. (1996) *EMBO J.* **15,** 3256–3266
16. Beinert, D., Neumann, L., Uebel, S., and Tampé, R. (1997) *Biochemistry* **36,** 4694–4700
17. Galocha, B., Hill, A., Barnett, B. C., Dolan, A., Raimondi, A., Cook, R. F., Brunner, J., McGeoch, D. J., and Ploegh, H. L. (1997) *J. Exp. Med.* **185,** 1565–1572
18. Neumann, L., Kraas, W., Uebel, S., Jung, G., and Tampé, R. (1997) *J. Mol. Biol.* **272,** 484–492
19. Bechinger, B., Aisenbrey, C., and Bertani, P. (2004) *Biochim. Biophys. Acta* **1666,** 190–204
20. Davis, J. H., and Auger, M. (1999) *Progress in NMR Spectroscopy* **35,** 1–84
21. Luca, S., Heise, H., and Baldus, M. (2003) *Acc. Chem. Res.* **36,** 858–865
22. Watts, A. (1999) *Curr. Opin. Biotechnol.* **10,** 48–53
23. Bechinger, B., and Sizun, C. (2003) *Concepts in Magnetic Resonance Part A* **18,** 130–145
24. Aisenbrey, C., and Bechinger, B. (2004) *Biochemistry* **43,** 10502–10512
25. Aisenbrey, C., and Bechinger, B. (2004) *J. Am. Chem. Soc.* **126,** 16676–16683
26. Gorbulev, S., Abele, R., and Tampé, R. (2001) *Proc. Natl. Acad. Sci. U. S. A.* **98,** 3732–3737
27. Chen, M., Abele, R., and Tampé, R. (2003) *J. Biol. Chem.* **278,** 29686–29692
28. Pfänder, R., Neumann, L., Zweckstetter, M., Seger, C., Holak, T. A., and Tampé, R. (1999) *Biochemistry* **38,** 13692–13698
29. Bechinger, B., Kinder, R., Helmle, M., Vogt, T. C., Harzer, U., and Schinzel, S. (1999) *Biopolymers* **51,** 174–190
30. Bechinger, B., and Opella, S. J. (1991) *J. Magn. Reson.* **95,** 585–588
31. Pines, A., Gibby, M. G., and Waugh, J. S. (1973) *J. Chem. Phys.* **59,** 569–590
32. Levitt, M. H., Suter, D., and Ernst, R. R. (1986) *J. Chem. Phys.* **84,** 4243–4255
33. Davis, J. H., Jeffrey, K. R., Bloom, M., Valic, M. I., and Higgs, T. P. (1976) *Chem. Phys. Lett.* **42,** 390–394
34. Teng, Q., and Cross, T. A. (1989) *J. Magn. Reson.* **85,** 439–447
35. Ducarme, P., Rahman, M., and Brasseur, R. (1998) *Proteins* **30,** 357–371
36. Kyte, J., and Doolittle, R. F. (1982) *J. Mol. Biol.* **157,** 105–132
37. Schwyzer, R. (1995) *Biopolymers* **37,** 5–16
38. Koradi, R., Billeter, M., and Wüthrich, K. (1996) *J. Mol. Graph.* **14,** 51–55